

Probing late-time annihilations of oscillating asymmetric dark matter via rotation curves of galaxies

Júlia G. Mamprim^{1*}, Guillermo Gambini^{1,2}, Luan B. Arbeletche¹,
Marcos Olegario¹, Vitor de Souza¹

^{1*}Instituto de Física de São Carlos, Universidade de São Paulo, Av. Trabalhador
São-carlense 400, São Carlos, 13566-590, São Paulo, Brazil.

²Facultad de Ciencia, Universidad Nacional de Ingenieria (UNI), Av. Túpac Amaru 210,
Lima, 15032, Perú.

*Corresponding author(s). E-mail(s): juliagouveamamprim@usp.br;

Abstract

In this paper, we explore the Oscillating Asymmetric Dark Matter (OADM) model to address the core-cusp problem, aiming to resolve the discrepancy between the predictions of the Λ CDM cosmological model and the observed dark matter profiles in dwarf spheroidal galaxies. The reactivation of dark matter annihilation during the structure formation epoch is possible if there is a small Majorana mass term that breaks the conservation of dark matter particle number, leading to oscillations between dark matter and its antiparticle. We analyzed the effects of the annihilation mechanism in the galaxy rotation curves of the SPARC and LITTLE THINGS catalogs. We searched for the characteristics of the OADM model which best describes the data. Our results show that the OADM model can successfully turn originally cusp-type halos into core-type ones according to our data sample.

Keywords: Dark matter, Asymmetric dark matter, Rotation curves, Core-cusp problem

1 Introduction

The nature of Dark Matter (DM) remains one of the most fundamental unsolved questions in physics. Numerous observations across different scales provide strong evidence for the presence of DM, including galaxy rotation curves [1], the dynamics of galaxy clusters [2], fluctuations in the cosmic microwave background [3], baryon acoustic oscillations [4], among others. However, the exact nature of Dark Matter remains unclear due to the lack of results from both direct detection experiments [5, 6] and indirect detection studies [7–10].

In 1970, Rubin and Ford [11] conducted the first precise measurement of the rotation curve of the Andromeda galaxy (M31) and found that the velocity profile was almost flat at large radii. This unexpected result suggested the abundance of dark matter within M31 and was later corroborated by observations of dozens of other galaxies. Despite providing intuitive evidence for the existence of dark matter, it is currently a challenge to conceal the observed rotation curves to theoretical aspects of the dark matter, in particular, their density profiles.

Several models attempt to describe the distribution of dark matter in galaxies, including the Navarro-Frenk-White (NFW) [12], Moore [13] and

Einasto [14] halo density profiles, among others. These models were developed using N-body simulations based on the Λ CDM cosmological framework, without accounting for baryonic feedback, and suggest a steep DM distribution in the central region of galaxies. However, observations of late-type dwarf galaxies, which are dominated by dark matter, reveal a roughly constant DM density at small radii. This discrepancy is known as the “core/cusp problem” [15, 16]. Including baryonic feedback in N-body simulations could potentially flatten the central cusps of halos in massive galaxies. However, it remains uncertain whether this solution is effective in the lowest mass galaxies, where such discrepancies are observed [17], or in systems like dwarf spheroidal galaxies, which have relatively low baryonic content.

Self-Interacting Dark Matter (SIDM) models present another potential solution to the core/cusp problem. Early SIDM simulations required scattering cross sections around $\sigma/m_\chi \sim (0.4 - 5) \text{ cm}^2/\text{g}$ [18, 19]. For small structures like dwarf spheroidal galaxies, removing dark matter cusps using SIDM models requires cross sections $> 1 \text{ cm}^2/\text{g}$ at $v_\chi \sim 10 \text{ km/s}$ [20] while most stringent constraints from merging galaxy clusters suggest $\sigma/m_\chi < 0.1 \text{ cm}^2/\text{g}$ [21]. SIDM models with velocity-dependent scattering cross-section that decreases with increasing velocity [22] could still make SIDM a viable solution to the core-cusp problem.

Our work directly builds off of reference [23], where it was shown, for representative benchmarks, that late-time dark matter annihilations in galactic structures could be responsible for erasure of the cusps in galactic dark matter density profiles while being allowed by CMB constraints [24, 25]. We perform a wider search of parameter space by fitting 37 rotation curves of galaxies using observational data from SPARC [26] and LITTLE THINGS [27], which have been selected for their high-quality rotation curves and high mass-to-light ratios. Our results demonstrate that the preferred window for the parameter space of fermionic OADM annihilating into a lighter scalar is the mass range [100-1000] MeV and dark fine structure constant α' around 0.1. Moreover, we find $\sigma/m_\chi \approx 0.06 \text{ cm}^2/\text{g}$ for the annihilation cross section is preferred by the χ^2 minimization and it presents very little scatter.

In Section 2, we define the OADM model framework. Section 3 describes how density profiles evolve from cusp-type to core-type within our model. Section 4 discusses the observational data and the methodology for fitting rotation velocity curves. Section 5 presents the results of the combined fits. Finally, Section 6 summarizes the findings and concludes the work.

2 Oscillating asymmetric dark matter formalism

We consider a dark matter field χ that is a quasi-Dirac fermion with mass m_χ . In this model, the DM couples to a complex scalar $\Phi = \phi + ia$, with effective Lagrangian

$$\mathcal{L} \supset -\frac{1}{2}m_\phi^2\phi^2 - \frac{1}{2}m_a^2a^2 - g'\bar{\chi}(\phi + ia\gamma_5)\chi, \quad (1)$$

where g' denotes the coupling between the DM particle and the scalar boson, with an associated dark fine-structure constant $\alpha' = g'^2/4\pi$. Dark matter freeze-out and late-time depletion are both allowed by the s -wave process $\chi\bar{\chi} \rightarrow a\phi$ (which, unlike the p -wave channels $\chi\bar{\chi} \rightarrow \phi\phi$ and $\chi\bar{\chi} \rightarrow aa$, is not suppressed at low velocities).

The mass term that permits DM-number violation is

$$\mathcal{L}_m = \frac{1}{2}\delta m(\bar{\chi}\chi^c + \text{H.c.}), \quad (2)$$

with the Majorana mass δm determining the timescale on which annihilations recouple after the freeze-out. The parameter δm must be small enough so that the oscillations between DM and its antiparticle have not yet started at the time of freeze-out. For a flavor-blind interaction, where scattering does not play a role as this type of interaction does not distinguish between χ and $\bar{\chi}$, annihilations start when oscillations repopulate the symmetric dark matter density, i.e., for $t \gtrsim \delta m^{-1}$ [28, 29]. Moreover, the oscillations should start before structure formation, $t_s \sim 0.1 \text{ Gyr}$ for annihilations to recouple during that epoch. However, if the annihilations are reactivated too early, the changes on DM relic density would be ruled out by CMB constraints [24, 25]. Taking the fractional change in the DM number density as $\delta_\eta \sim 3\%$ (limited by the change in the dark matter

density after the formation of the CMB), and considering $m_\chi \sim 100$ MeV, an approximate window of values for δm can be set [23]:

$$\frac{1}{t_s} \lesssim \delta m \lesssim 3 \times 10^{-30} \text{ eV}. \quad (3)$$

Eur. Phys. J. C manuscript No. Above $m_\chi \sim 1$ GeV, the theory starts to be strongly coupled [23], so we restrain our analysis to this maximum mass value.

The annihilation cross section at threshold, *i.e.* the minimum energy at which the annihilation process can occur, reads

$$\langle \sigma v \rangle_a = \frac{\pi \alpha'^2}{m_\chi^2} \left(1 - \frac{m_\phi^2}{4m_\chi^2} \right), \text{Eur. Phys. J. C manuscript No.} \quad (4)$$

where we have assumed, for simplicity, the following hierarchy $m_a \ll m_\phi$, and neglected the suppressed channels $\chi\bar{\chi} \rightarrow \phi\phi$ and $\chi\bar{\chi} \rightarrow aa$.

Even though $\chi\chi$ elastic scatterings are irrelevant for the reactivation of dark matter annihilations at late times when the interaction is flavor-blind, as in this model, we consider values in the parameter space for which DM annihilations are dominant over scattering self-interactions which, otherwise, could change the DM density profiles in the center of galaxies as in SIDM models.

When DM oscillations are present, the difference between particle and antiparticle varies over time. For interactions that don't distinguish between a dark matter particle and its antiparticle, the evolution of the DM and anti-DM number densities, encoded in the 2 by 2 matrix n , is best described by the Boltzmann equation [29]

$$\dot{n} + 3Hn = -i[H_0, n] - \langle \sigma v \rangle_a \times \left[\begin{pmatrix} \det' n & (\text{Tr} n) n_{12} \\ (\text{Tr} n) n_{21} & \det' n \end{pmatrix} - n_{\text{eq}}^2 \mathbb{1} \right], \quad (5)$$

where H is the Hubble parameter, n_{eq} is the equilibrium number density, and $\det' \equiv n_{11}n_{22} + n_{12}n_{21}$. As an approximation, we considered the DM density to be spatially homogeneous and isotropic for an already formed DM halo, simplifying the terms that come from the Liouville operator in the Boltzmann equation [30]. In that sense, the diffusion of dark matter particles in the system is not considered by this approach.

However, N-body simulations show close results to the Boltzmann method [23], but this analysis is outside the scope of this work.

Ref. [23] also describes another DM model, with a vector mediator and flavor-sensitive interactions. In contrast to the scalar model, the Boltzmann equation for the flavor-sensitive case presents a dependence on the DM velocity, which could lead to different levels of change in the halo density profiles depending on the size of the galactic system considered. Since we are performing a combined analysis based on data from two distinct rotation curves catalogs, with galaxies that vary in extension, it is a reasonable choice to probe only the scalar model's parameters through this method.

3 A model for halo density profile evolution with OADM

To test the effect of the flavor-blind OADM model on galaxy rotation curves, we consider an initial NFW-shaped dark matter halo, already formed at time t_0 [12]:

$$\rho_{\text{NFW}, t_0} = \frac{\rho_s}{(r/r_s)(1+r/r_s)^2}, \quad (6)$$

where r_s is the scale radius of the system, and ρ_s is the scale density $\rho_s = \rho_c \delta_c$, given as a function of the critical density of the Universe ρ_c and an over density parameter $\delta_c = (200/3)(c_{200}^3/f(c_{200}))$. Here, c_{200} is the concentration parameter, defined from the Virial radius r_{200} as $c_{200} = r_{200}/r_s$, and $f(c_{200})$ corresponds to the function $f(c_{200}) = \ln(1+c_{200}) - c_{200}/(1+c_{200})$.

Before the oscillations have any effect on the collapsed halo environment, the initial condition at each position r for the density matrix is

$$n_{ij}(r; t_0) = \frac{\rho_{\text{NFW}, t_0}(r)}{m_\chi} \delta_{i1} \delta_{j1}, \quad (7)$$

which represents a pure dark matter χ state.

For a galactic halo, where the expansion of the universe can be safely neglected, equation 5 simplifies by dropping the $3Hn$ term and the equilibrium function since $n_{\text{eq}} \rightarrow 0$ at late times. Furthermore, since NFW profiles vary orders of magnitude from the inner part of a galaxy to its outskirts, we can assume the products of the annihilations can escape from the galactic system without interacting again.

Under these assumptions, we evolve the initial density matrix 7 at each radial position r from $t_0 \sim 0.1\text{Gyr}$ until $t_f \sim 10\text{Gyr}$ [22, 23], leading to a modified density profile $\rho_\chi(t_f) = (n_{11}(t_f) + n_{22}(t_f))m_\chi$ that we compare to observational data.

4 Fitting measured galaxy rotation curves

To probe the parameter space of the aforementioned OADM model, we utilized observed rotation curves of 37 galaxies from two different database catalogs, namely SPARC (Spitzer Photometry & Accurate Rotation Curves) [26] and LITTLE THINGS (Local Irregulars That Trace Luminosity Extremes, The HI Nearby Galaxy Survey) [27].

SPARC is a sample of 175 late-type galaxies with high-quality HI/H α rotation curves and near-infrared Spitzer photometry. The morphologies vary among spirals and irregulars, presenting a wide range in stellar masses, surface brightnesses, and gas fractions. The mass distribution for stellar disk and bulge is traced with Spitzer photometry at $3.6\mu\text{m}$, and the mass contribution of the gas is derived from the observed HI surface density profile, scaled up to include Helium [31].

A high baryonic component in the galactic environment could lead to effects that we did not consider in our model, such as baryonic feedback and more expressive non-circular contributions to the galaxy motion. Therefore, we made a conservative cut in the SPARC sample, selecting only the 18 galaxies that have a mass-to-light ratio larger than $4M_\odot/L_\odot$. All of the selected galaxies do not present a clear bulge region (a dense, spherical region of stars located at the center of many spiral galaxies), and are described only by gas, disk and halo components.

The LITTLE THINGS sample includes 37 dwarf irregular (dIm) and 4 Blue Compact Dwarf (BCD) galaxies. A subset of 26 galaxies that show regular rotation pattern in their two-dimensional HI velocity fields had their rotation curves and mass models derived in Ref. [32] from the high-resolution HI observations, complemented with Spitzer $3.6\mu\text{m}$ measurements, as well as H α , optical U, B, V and near-infrared images. Among those 26, we excluded three galaxies

(DDO50, IC10, IC1613) that presented high baryonic gas content and other three galaxies (DDO46, DDO101, NGC3738) that had an isothermal halo profile scale density $\rho_0 \gtrsim 500 \times 10^{-3}M_\odot\text{pc}^{-3}$ [32], because a very high initial scale density could lead annihilations to be too efficient, with the total density profile vanishing at the timescales ($\sim 10\text{Gyr}$) we are working with. It is important to emphasize that the model's mechanism is effective for the systems in question but only within shorter evolution intervals ($\sim 5\text{Gyr}$). This limitation may suggest that these halos have not yet reached equilibrium, with their concentration parameters still evolving toward their final values. To avoid introducing the evolution time of the systems as an additional parameter in the fit, we opted to exclude these outlier galaxies from the analysis. Therefore, after the quality cuts, we were left with 20 galaxies from the LITTLE THINGS catalog.

The rotation curves from both samples were compared to the rotation velocity curves obtained by integrating our modified density profile ρ_{χ,t_f} ,

$$V_\chi^2(r) = \frac{GM(r)}{r} = \frac{4\pi G}{r} \int_0^r r'^2 \rho_{\chi,t_f}(r') dr'. \quad (8)$$

The contribution of each galactic component is accounted by the relation

$$V_{\text{tot}}^2 = V_\chi^2 + \Upsilon_\star V_\star^2 + V_{\text{gas}}^2, \quad (9)$$

where V_{tot} is the total velocity expected after evolving the initial density profile, V_χ is the dark matter halo component, V_\star is the stellar disk contribution, V_{gas} comprise the gas fraction, and Υ_\star is the stellar mass-to-light ratio. While the mass of the gas component can be directly estimated from HI observations, the stellar mass in galaxies is strongly dependent on the assumed Υ_\star , which is usually responsible for the largest uncertainties when converting the luminosity profile to the mass density profile [26]. For SPARC and LITTLE THINGS galaxies, respectively, we took the Υ_\star values as discussed in Ref. [26] and Ref. [32].

The free parameters of our model are adjusted to minimize the χ^2 statistic, defined as

$$\chi^2 = \sum_{r_i} \frac{[V_{\text{obs}}(r_i) - V_{\text{tot}}(r_i)]^2}{\sigma_i^2}, \quad (10)$$

where V_{obs} is the observed rotation velocity, σ_i is the observational uncertainty and V_{tot} is the total

rotation velocity expected after evolving the initial density profile. We perform a grid-search over the $\alpha' \times m_\chi$ parameter space for 50 linearly spaced steps in the ranges $[0.01, 0.3]$ and $[100.0, 1000.0]$ MeV, respectively. For each pair (α', m_χ) , we fit the observations to a NFW-profile, with two free parameters: the halo scale radius r_s and the scale density ρ_s .

Figures 1 and 3 show the result of the fit for NGC3109 in the SPARC catalog and for DDO154 in the LITTLE THINGS catalog, respectively, as an example. Figures 2 and 4 show the corresponding evolution of the halo density profile of these galaxies. On Table 1, we present the best-fit parameters corresponding to the minimum χ_{red}^2 in the $\alpha' \times m_\chi$ grid, where $\chi_{\text{red}}^2 = \frac{\chi^2}{n-m}$ is the reduced χ^2 , with n being the number of observations, and m the number of fitted parameters. We see that, in the grid-search, a good fit was found for all the galaxies in our sample.

The first two parameters in our model, r_s and ρ_s , come from the initial NFW halo density profile, and are expected to differ from one galaxy to another. The parameters m_χ and α' , on the other hand, relate to the OADM model and should, in principle, be the same for all galaxies. By fitting these parameters individually for each galaxy, however, we did not verify this last statement. Therefore, in order to explore the pair of parameters m_χ and α' that best describe our ensembles of galaxies, a combined approach is necessary, which is presented in the next section.

5 Results of the fit for the catalogs of galaxies

We have searched the $\alpha' \times m_\chi$ parameter space following the procedure described in Section 4, for all galaxies in our sample. The resulting minimized statistic χ_{tot}^2 is given, then, by the sum over individual galaxies $\chi_{\text{tot}}^2 = \sum_{i=1}^N \chi_{\text{red},i}^2$, where N is the ensemble size. We work with χ_{red}^2 instead of χ^2 to account for the fact that the number of observations is different for each galaxy. The procedure is executed for three different groups of galaxies: SPARC, LITTLE THINGS, and both. Figures 5, 6, and 7 show the obtained maps of χ_{tot}^2 in the $\alpha' \times m_\chi$ for each of the three groups.

The behaviour of the minimum of χ_{tot}^2 shows the relation between m_χ and α' . Through this

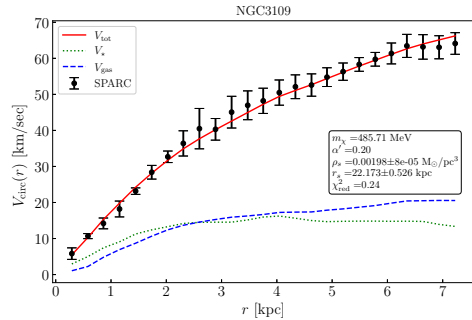


Fig. 1 Rotational velocity as a function of the distance from the center. Box shows the result of the NFW profile with OADM model for the galaxy NGC3109, with fixed values for $\delta m = 1.0 \times 10^{-31}$ and $m_\phi = 0.7m_\chi$. The black dots show the observational rotation velocity data available in the SPARC catalog. The green dotted line is the gas component, and the blue dashed line is the stellar disk component, both given by SPARC. The red line is the result of the fit for V_{tot} . The reduced χ^2 is given by $\chi_{\text{red}}^2 = \frac{\chi^2}{n-m}$, where n equals the number of observations, and m is the number of fitted parameters.

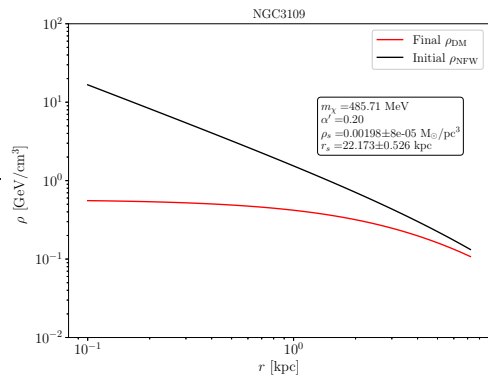


Fig. 2 Dark matter density as a function of the distance from center for the galaxy NGC3109, with fixed values for $\delta m = 1.0 \times 10^{-31}$ and $m_\phi = 0.7m_\chi$. The black line is the initial NFW profile, with ρ_s and r_s as shown in the figure. The red line shows the final density profile, affected by the annihilations in the OADM model.

relation, it is possible to estimate the value of σ/m_χ for the annihilation process. We can write an equation analogous to 4

$$\frac{\sigma}{m_\chi} = \frac{\pi}{v_0} \left(1 - \frac{r^2}{4} \right) \frac{\alpha'^2}{m_\chi^3}, \quad (11)$$

where v_0 is a reference velocity for DM in a galactic halo and $r_m \equiv m_\phi/m_\chi$. Writing α' as a function of m_χ gives

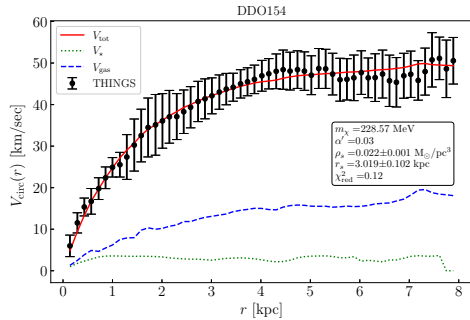


Fig. 3 Rotational velocity as a function of the distance from the center. Box shows the result of the NFW profile with OADM model for the galaxy DDO154, with fixed values for $\delta m = 1.0 \times 10^{-31}$ and $m_\phi = 0.7m_\chi$. The black dots show the observational rotation velocity data available in the LITTLE THINGS catalogue. The green dotted line is the gas component, and the blue dashed line is the stellar disk component, both given by LITTLE THINGS. The red line is the result of the fit for V_{tot} . The reduced χ^2 is given by $\chi_{\text{red}}^2 = \frac{\chi^2}{n-m}$, where n equals the number of observations, and m is the number of fitted parameters.

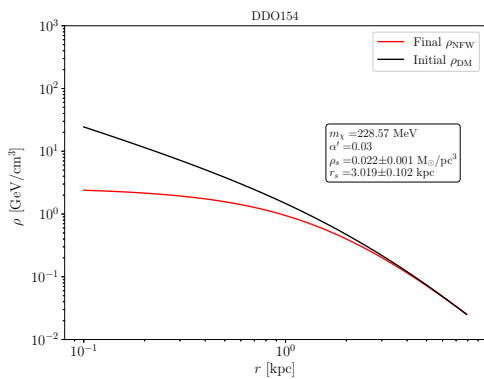


Fig. 4 Dark matter density as a function of the distance from center for the galaxy DDO154, with fixed values for $\delta m = 1.0 \times 10^{-31}$ and $m_\phi = 0.7m_\chi$. The black line is the initial NFW profile, with ρ_s and r_s as shown in the figure. The red line shows the final density profile, affected by the annihilations.

$$\alpha' = \beta \left(\frac{\sigma}{m_\chi} \right)^{1/2} m_\chi^{3/2}, \quad (12)$$

with $\beta = [v_0/\pi(1 - r_m^2/4)]^{1/2}$. The blue line in figures 5, 6 and 7 shows the fit of the function 12, where we assumed $v_0 = 100$ km/s, a value characteristic of DM in a Milky-Way-like galaxy.

The combined fit performed with LITTLE THINGS data reaches a minimum region more smoothly. This behavior could be explained by

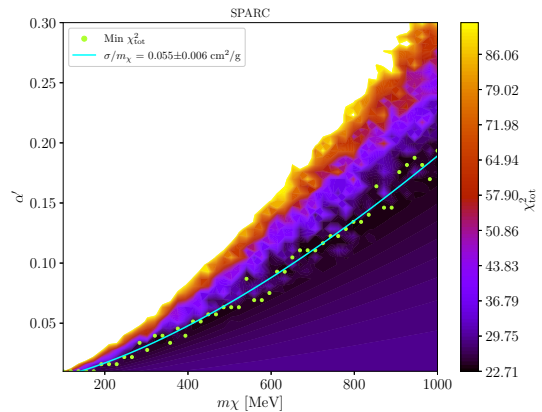


Fig. 5 Value of the χ_{tot}^2 in the $\alpha' \times m_\chi$ parameter space for the 18 galaxies from SPARC. The green markers correspond to the minimum of χ_{tot}^2 at discrete values of α' and m_χ . The blue line shows the fit with the function 12.

the homogeneity of galaxy morphologies in the LITTLE THINGS catalog, which is not true for SPARC. Also, LITTLE THINGS sample has, in general, more data points with large uncertainties for the rotation velocity curves when compared to SPARC. The result for the merge of both catalogs is closer to the one that considers SPARC alone, since the bumps of high-valued χ_{tot}^2 in SPARC fit dominate over the lower values of LITTLE THINGS.

The results for σ/m_χ are slightly small if compared to the SIDM scattering cross-sections, although for different choices of v_0 , they are comparable in order of magnitude with the ones found in Ref. [22]. For example, a lower DM velocity, characteristic of small systems, $v_0 = 20$ km/s gives $\sigma/m_\chi = (0.533 \pm 0.032) \text{cm}^2/\text{g}$ considering the LITTLE THINGS sample. The fits show that OADM successfully turned cusp-type halos into cored ones for all the galaxies in our sample, and the results do not depend on the mass of the mediator m_ϕ , in accordance with Ref. [23].

6 Conclusion

In this paper, we used observational data from galaxy rotation curves to probe the Oscillating Asymmetric Dark Matter (OADM) model with a fermionic dark matter particle coupling to a complex scalar. In this model, a small Majorana mass

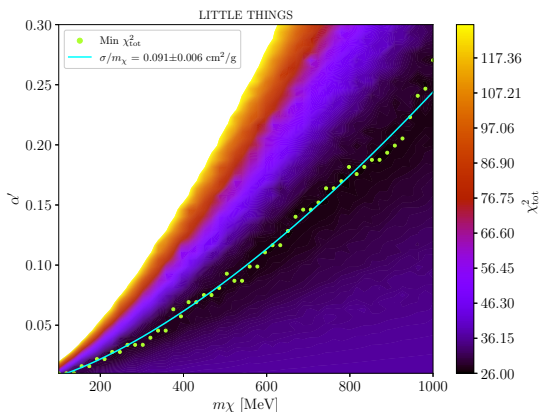


Fig. 6 Value of the χ_{tot}^2 in the $\alpha' \times m_\chi$ parameter space for the 20 galaxies from LITTLE THINGS. The green markers correspond to the minimum of χ_{tot}^2 at discrete values of α' and m_χ . The blue line shows the fit with the function 12..

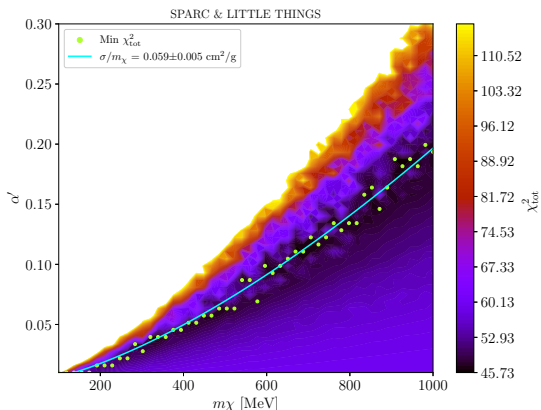


Fig. 7 Value of the χ_{tot}^2 in the $\alpha' \times m_\chi$ parameter space for 37 galaxies from SPARC and LITTLE THINGS together. Galaxy DDO154 appears in both catalogues, and we chose to use LITTLE THINGS data since it presented more data points. The green markers correspond to the minimum of χ_{tot}^2 at discrete values of α' and m_χ . The blue line shows the fit with the function 12.

term violates the conservation of dark matter particle number, leading to oscillations between dark matter and its antiparticle. After freeze-out, these oscillations recouple during the time of structure formation and may transform cusp-type halo density profiles into cored profiles, offering a solution to the core/cusp problem.

We analyzed data from two different rotation curve catalogs: SPARC and LITTLE THINGS. The former includes a more diverse sample in terms of galaxy morphology, while the latter focuses exclusively on dwarf galaxies. The observed rotation curves were compared to those predicted by the OADM model after evolving an initial NFW density profile over 10 Gyr using an analysis based on solving the Boltzmann equations for the dark matter number density from an initial NFW profile. The fit results demonstrate that the cusp-type profiles were effectively transformed into a cored profiles for all the galaxies in our sample. Although the individual fits for each galaxy return varying preferred values of α' and m_χ , the combined fits show that it is possible to successfully find values that work well for all galaxies together.

A complementary analysis using N-body simulations could strengthen our results since it has been shown that their results are close to the one obtained by the quantum Boltzmann approach [23]. The simulations could, for example, explore scenarios where the DM elastic self-scattering cross section is sizable to the annihilation cross section, the latter of which we have assumed to be dominant. We defer this study for future work. Finally, there remains much phenomenology to be explored with ADM oscillations, which could lead to potential indirect detection signals from the annihilations [29, 33]

Acknowledgments

Authors are supported by the São Paulo Research Foundation (FAPESP) through grants number 2021/01089-1 and 2022/16842-0. VdS is supported by CNPq through grant number 308837/2023-1. GG acknowledges support from Universidad Nacional de Ingeniería funding Grant FC-PFR-42-2024. The authors acknowledge the National Laboratory for Scientific Computing (LNCC/MCTI, Brazil) for providing HPC resources for the SDumont supercomputer (<http://sdumont.lncc.br>).

This version of the article has been accepted for publication, after peer review (when applicable) but is not the Version of Record and does not reflect post-acceptance improvements, or any corrections. The Version of Record is available

online at: <http://dx.doi.org/10.1140/epjc/s10052-025-13875-x>.

Table 1 The best-fit parameters r_s and ρ_s corresponding to the minimum χ_{red}^2 in the $\alpha' \times m_\chi$ grid, for each galaxy.

Catalog/Galaxy	α'	m_χ [MeV]	ρ_s [$\times 10^{-2} M_\odot/\text{pc}^3$]	r_s [kpc]	χ_{red}^2
SPARC					
DDO154	0.152	448.979	5.28 ± 1.12	2.15 ± 0.21	0.9
DDO170	0.229	1000.0	0.85 ± 0.24	5.95 ± 0.93	1.1
ESO444-G084	0.022	632.653	0.30 ± 0.08	11.35 ± 2.38	0.1
F563-V2	0.264	889.796	33.85 ± 5.54	1.60 ± 0.13	0.1
F565-V2	0.016	100.0	0.76 ± 0.11	9.51 ± 0.85	0.1
F568-V1	0.069	375.510	29.63 ± 13.24	1.92 ± 0.35	0.1
NGC3109	0.199	485.741	0.10 ± 0.01	2.17 ± 0.53	0.2
UGC00128	0.010	853.061	0.41 ± 0.03	16.39 ± 0.84	2.8
UGC00731	0.199	908.163	2.60 ± 0.57	3.82 ± 0.42	0.3
UGC00891	0.069	559.184	0.11 ± 0.06	27.25 ± 13.89	0.9
UGC05716	0.010	283.673	0.61 ± 0.08	7.85 ± 0.64	1.9
UGC05764	0.039	283.673	70.73 ± 17.83	0.77 ± 0.09	3.0
UGC05829	0.010	118.367	0.24 ± 0.01	13.56 ± 0.57	0.1
UGC05918	0.016	173.469	0.79 ± 0.47	6.05 ± 2.61	0.6
UGC06667	0.282	889.796	7.85 ± 0.85	3.11 ± 0.17	0.1
UGC07608	0.205	761.224	0.75 ± 0.25	7.72 ± 1.79	0.1
UGCA442	0.259	742.857	1.81 ± 0.60	4.06 ± 0.70	0.6
UGCA444	0.051	320.408	1.02 ± 0.48	3.82 ± 1.12	0.2
LITTLE THINGS					
CVnidwa	0.294	467.347	16.38 ± 8.95	2.26 ± 0.31	1.7
DDO43	0.270	761.224	11.66 ± 5.45	1.10 ± 0.21	0.5
DDO47	0.300	595.918	3.96 ± 0.35	4.26 ± 0.20	4.9
DDO52	0.247	889.796	3.52 ± 1.09	3.32 ± 0.53	0.1
DDO53	0.193	614.286	13.85 ± 6.59	1.19 ± 0.27	0.7
DDO70	0.010	155.102	0.46 ± 0.16	8.62 ± 2.45	1.4
DDO87	0.294	761.224	0.22 ± 0.05	13.59 ± 1.97	0.2
DDO126	0.176	504.082	9.02 ± 1.35	1.41 ± 0.07	0.3
DDO133	0.075	448.979	0.06 ± 1.35	1.90 ± 0.22	0.8
DDO154	0.028	228.571	2.23 ± 0.13	3.02 ± 0.10	0.1
DDO168	0.140	540.816	13.30 ± 7.02	2.90 ± 0.39	2.1
DDO210	0.028	283.673	1.53 ± 0.36	1.78 ± 0.54	0.3
DDO216	0.010	283.673	2.12 ± 1.26	0.97 ± 0.37	0.2
F564-V3	0.093	448.979	28.83 ± 14.53	0.72 ± 0.18	1.6
HARO29	0.045	926.531	4.64 ± 1.29	1.46 ± 0.21	0.3
HARO36	0.229	724.490	0.37 ± 0.20	18.80 ± 7.54	0.2
NGC1569	0.193	577.551	2.74 ± 0.33	3.40 ± 0.39	0.1
NGC2366	0.069	338.775	13.27 ± 0.87	1.58 ± 0.04	0.1
UGC8508	0.111	522.449	0.75 ± 0.03	13.72 ± 0.47	0.2
WLM	0.241	889.796	76.32 ± 18.56	0.45 ± 0.04	1.5

References

- [1] Sofue, Y., Rubin, V.: Rotation curves of spiral galaxies. *Ann. Rev. Astron. Astrophys.* **39**, 137–174 (2001) <https://doi.org/10.1146/annurev.astro.39.1.137>
- [2] Clowe, D., Bradac, M., Gonzalez, A.H., Markevitch, M., Randall, S.W., Jones, C., Zaritsky, D.: A direct empirical proof of the existence of dark matter. *Astrophys. J. Lett.* **648**, 109–113 (2006) <https://doi.org/10.1086/508162>
- [3] Aghanim, N., *et al.*: Planck 2018 results. VI. Cosmological parameters. *Astron. Astrophys.* **641**, 6 (2020) <https://doi.org/10.1051/0004-6361/201833910>. [Erratum: *Astron. Astrophys.* 652, C4 (2021)]
- [4] Eisenstein, D.J., *et al.*: Detection of the Baryon Acoustic Peak in the Large-Scale Correlation Function of SDSS Luminous Red Galaxies. *Astrophys. J.* **633**, 560–574 (2005) <https://doi.org/10.1086/466512>
- [5] Akerib, D.S., *et al.*: Results from a search for dark matter in the complete LUX exposure. *Phys. Rev. Lett.* **118**(2), 021303 (2017) <https://doi.org/10.1103/PhysRevLett.118.021303>
- [6] Arcadi, G., Dutra, M., Ghosh, P., Lindner, M., Mambrini, Y., Pierre, M., Profumo, S., Queiroz, F.S.: The waning of the WIMP? A review of models, searches, and constraints. *Eur. Phys. J. C* **78**(3), 203 (2018) <https://doi.org/10.1140/epjc/s10052-018-5662-y>
- [7] Abdallah, H., *et al.*: Search for γ -Ray Line Signals from Dark Matter Annihilations in the Inner Galactic Halo from 10 Years of Observations with H.E.S.S. *Phys. Rev. Lett.* **120**(20), 201101 (2018) <https://doi.org/10.1103/PhysRevLett.120.201101>
- [8] Abdallah, H., *et al.*: Search for dark matter annihilations towards the inner Galactic halo from 10 years of observations with H.E.S.S. *Phys. Rev. Lett.* **117**(11), 111301 (2016) <https://doi.org/10.1103/PhysRevLett.117.111301>
- [9] Ahnen, M.L., *et al.*: Limits to Dark Matter Annihilation Cross-Section from a Combined Analysis of MAGIC and Fermi-LAT Observations of Dwarf Satellite Galaxies. *JCAP* **02**, 039 (2016) <https://doi.org/10.1088/1475-7516/2016/02/039>
- [10] Oakes, L., *et al.*: Combined Dark Matter searches towards dwarf spheroidal galaxies with *Fermi*-LAT, HAWC, HESS, MAGIC and VERITAS. *PoS ICRC2019*, 012 (2021) <https://doi.org/10.22323/1.358.0012>
- [11] Rubin, V.C., Ford, J. W. Kent: Rotation of the Andromeda Nebula from a Spectroscopic Survey of Emission Regions. *Astrophysical Journal* **159**, 379 (1970) <https://doi.org/10.1086/150317>
- [12] Navarro, J.F., Frenk, C.S., White, S.D.M.: The structure of cold dark matter halos. *The Astrophysical Journal* **462**, 563 (1996) <https://doi.org/10.1086/177173>
- [13] Moore, B., Governato, F., Quinn, T.R., Stadel, J., Lake, G.: Resolving the structure of cold dark matter halos. *Astrophys. J. Lett.* **499**, 5 (1998) <https://doi.org/10.1086/311333>
- [14] Einasto, J.: On the Construction of a Composite Model for the Galaxy and on the Determination of the System of Galactic Parameters. *Trudy Astrofizicheskogo Instituta Alma-Ata* **5**, 87–100 (1965)
- [15] Blok, W.J.G.: The core-cusp problem. *Advances in Astronomy* **2010**(1) (2009) <https://doi.org/10.1155/2010/789293>
- [16] Salucci, P.: The distribution of dark matter in galaxies. *Astron. Astrophys. Rev.* **27**(1), 2 (2019) <https://doi.org/10.1007/s00159-018-0113-1>
- [17] Weinberg, D.H., Bullock, J.S., Governato,

- F., Naray, R., Peter, A.H.G.: Cold dark matter: controversies on small scales. *Proc. Nat. Acad. Sci.* **112**, 12249–12255 (2015) <https://doi.org/10.1073/pnas.1308716112>
- [18] Spergel, D.N., Steinhardt, P.J.: Observational evidence for self-interacting cold dark matter. *Phys. Rev. Lett.* **84**, 3760–3763 (2000) <https://doi.org/10.1103/PhysRevLett.84.3760>
- [19] Tulin, S., Yu, H.-B.: Dark Matter Self-interactions and Small Scale Structure. *Phys. Rept.* **730**, 1–57 (2018) <https://doi.org/10.1016/j.physrep.2017.11.004>
- [20] Eckert, D., Ettori, S., Robertson, A., Massey, R., Pointecouteau, E., Harvey, D., McCarthy, I.G.: Constraints on dark matter self-interaction from the internal density profiles of X-COP galaxy clusters. *Astron. Astrophys.* **666**, 41 (2022) <https://doi.org/10.1051/0004-6361/202243205>
- [21] Markevitch, M., Gonzalez, A.H., Clowe, D., Vikhlinin, A., David, L., Forman, W., Jones, C., Murray, S., Tucker, W.: Direct constraints on the dark matter self-interaction cross-section from the merging galaxy cluster 1E0657-56. *Astrophys. J.* **606**, 819–824 (2004) <https://doi.org/10.1086/383178>
- [22] Kaplinghat, M., Tulin, S., Yu, H.-B.: Dark Matter Halos as Particle Colliders: Unified Solution to Small-Scale Structure Puzzles from Dwarfs to Clusters. *Phys. Rev. Lett.* **116**(4), 041302 (2016) <https://doi.org/10.1103/PhysRevLett.116.041302>
- [23] Cline, J.M., Gambini, G., McDermott, S.D., Puel, M.: Late-Time Dark Matter Oscillations and the Core-Cusp Problem. *JHEP* **04**, 223 (2021) [https://doi.org/10.1007/JHEP04\(2021\)223](https://doi.org/10.1007/JHEP04(2021)223)
- [24] Poulin, V., Serpico, P.D., Lesgourgues, J.: A fresh look at linear cosmological constraints on a decaying dark matter component. *JCAP* **08**, 036 (2016) <https://doi.org/10.1088/1475-7516/2016/08/036>
- [25] Bringmann, T., Kahlhoefer, F., Schmidt-Hoberg, K., Walia, P.: Converting nonrelativistic dark matter to radiation. *Phys. Rev. D* **98**(2), 023543 (2018) <https://doi.org/10.1103/PhysRevD.98.023543>
- [26] Lelli, F., McGaugh, S.S., Schombert, J.M.: SPARC: Mass Models for 175 Disk Galaxies with Spitzer Photometry and Accurate Rotation Curves. *Astron. J.* **152**, 157 (2016) <https://doi.org/10.3847/0004-6256/152/6/157>
- [27] Hunter, D.A., *et al.*: Little Things. *Astron. J.* **144**, 134 (2012) <https://doi.org/10.1088/0004-6256/144/5/134>
- [28] Kaplan, D.E., Luty, M.A., Zurek, K.M.: Asymmetric Dark Matter. *Phys. Rev. D* **79**, 115016 (2009) <https://doi.org/10.1103/PhysRevD.79.115016>
- [29] Tulin, S., Yu, H.-B., Zurek, K.M.: Oscillating Asymmetric Dark Matter. *JCAP* **05**, 013 (2012) <https://doi.org/10.1088/1475-7516/2012/05/013>
- [30] Kolb, E.W.: *The Early Universe* vol. 69. Taylor and Francis, ??? (2019). <https://doi.org/10.1201/9780429492860>
- [31] Li, P., Lelli, F., McGaugh, S., Schombert, J.: A comprehensive catalog of dark matter halo models for SPARC galaxies. *Astrophys. J. Suppl.* **247**(1), 31 (2020) <https://doi.org/10.3847/1538-4365/ab700e>
- [32] Oh, S.-H., *et al.*: High-resolution mass models of dwarf galaxies from LITTLE THINGS. *Astron. J.* **149**, 180 (2015) <https://doi.org/10.1088/0004-6256/149/6/180>

- [33] Petraki, K., Volkas, R.R.: Review of asymmetric dark matter. *Int. J. Mod. Phys. A* **28**, 1330028 (2013)
<https://doi.org/10.1142/S0217751X13300287>

